Journal of Materials Chemistry A

Accepted Manuscript

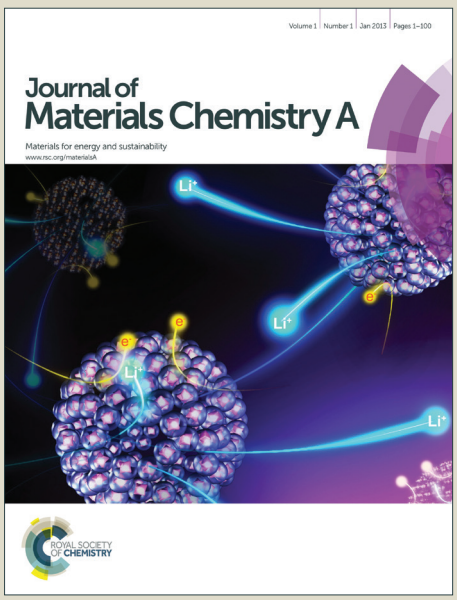

ROYAL SOCIETY OF CHEMISTRY

www.rsc.org/materialsA

Efficient Ternary Bulk Heterojunction Solar Cells Based on Small Molecules Only

Tzu-Yen Huang[a,b], Dhananjaya Patra[b], Yu-Sheng Hsiao[c], Sheng Hsiung Chang[d], Chun-Guey Wu[d], Kuo-Chuan Ho[a,e,*], Chih-Wei Chu[b,*]

[a] Department of Chemical Engineering, National Taiwan University, Taipei, Taiwan (R.O.C.) 10617

[b] Research Center for Applied Sciences, Academia Sinica, Taipei, Taiwan (R.O.C.) 11529

[c] Department of Materials Engineering, Mingchi University of Technology, New Taipei City, Taiwan (R.O.C.) 24301

[d] Research Center for New Generation Photovoltaics, Jhongli City, Taiwan (R.O.C.) 32001

[e] Institute of Polymer Science and Engineering, National Taiwan University, Taipei, Taiwan (R.O.C.) 10617

*Corresponding authors. E-mail: kcho@ntu.edu.tw (K.-C.H.); gchu@gate.sinica.edu.tw (C.-W.C.). Telephone: +886-2-23660739 (K.-C.H.); +886-2-27187523 (C.-W.C.). Fax: +886-2-23623040 (K.-C.H.); +886-2-27873122 (C.-W.C.).

Abstract

Ternary bulk heterojunctions (BHJs) are platforms that can improve the power conversion efficiencies of organic solar cells. In this paper, we report an all-small-molecule ternary BHJ solar cell incorporating [6,6]-phenyl-C_{71}-butyric acid methyl ester ($PC_{71}BM$) and indene-C_{60} bisadduct (ICBA) as mixed acceptors and the conjugated small molecule (2*Z*,2′*E*)-dioctyl 3,3′-(5′′,5′′′′′-(4,8-bis(5-octylthiophen-2-yl)benzo[1,2-*b*:5,4-*b*′]dithiophene-2,6-diyl) bis(3,4′,4′′-trioctyl-[2,2′:5′,2′′-terthiophene]-5′′,5-diyl))bis(2-cyanoacrylate) (BDT6T) as a donor. When incorporating a 15% content of ICBA relative to $PC_{71}BM$, the ternary BHJ solar cell reached a power conversion efficiency of 6.36% with a short-circuit current density (J_{SC}) of 12.00 mA cm^{-2}, an open-circuit voltage (V_{OC}) of 0.93 V, and a fill factor of 0.57. The enhancement in efficiency, relative to that of the binary system, resulted mainly from the increased value of J_{SC}, attributable to not only the better intermixing for the donor and acceptor that improved charge transfer but also the more suitable morphology for efficient dissociation of excitons and more effective charge extraction. Our results suggest that there is great potential for exceeding the efficiencies of binary solar cells through adding a third component, without sacrificing the simplicity of the fabrication process.

Keywords: solution-processing, small molecule, ternary, organic solar cells, fullerene

1. Introduction

Solution-processed organic solar cells (OSCs) are attractive as inexpensive renewable energy sources because of their low manufacturing costs and potential for fabrication in flexible large-area devices.[1-5] Steady progress in the development of conjugated polymers having donor/acceptor structures has resulted in the power conversion efficiencies (PCEs) reaching greater than 10% for single cells and greater than 11% for tandem cells, based on the most promising bulk heterojunction (BHJ) architecture.[6-9] Devices based on small molecules are also of interest because these small molecules can be solution-processed, just like polymers, while having the advantages of well-defined molecular structures, high purities without batch-to-batch variation, and high mobility.[10, 11] Nevertheless, solution-processed small-molecule organic solar cells (SMOSCs) usually exhibit low performance, due to poor film formation and discontinuous morphologies when applied in BHJ architectures.[12, 13] From a quest to design novel molecular structures, Nguyen et al. reported a diketopyrrolopyrrole-containing small molecule that could greatly improve the interconnectivity in a blend, leading to a PCE of 4.4%.[14] Since then, interest in solution-processed small molecules for use in OSCs has accelerated, with the PCEs of state-of-the-art SMOSCs having now exceeded 9%,[15, 16] thereby making them more competitive than their polymeric counterparts.

To prepare OSCs with sufficiently high PCEs for practical applications, research has been focused on the synthesis of materials having low band gaps,[17, 18] the development of new device configurations,[16, 19] and optimizing the fabrication conditions.[20, 21] Among new device configurations, the ternary blend is one of the most promising strategies for improving the performance of an OSC while retaining the simplicity of a single step for processing the active layer. To achieve efficient ternary BHJ solar cells, the additional material must have appropriate energy level

offsets with respect to its blend counterparts to allow efficient dissociation of excitons and decrease the energy barrier for carrier transfer. Most ternary blend systems in recent reports have featured two donor materials and one fullerene acceptor to improve the PCE. Several cascade materials, including polymers,[22-24] small molecules,[25-27] and quantum dots,[28, 29] have been incorporated to cover a wider range of the solar irradiation spectrum or to optimize the film morphology. In contrast, only a few papers have reported ternary systems based on one donor material and two fullerene acceptors.[30] Indene-C_{60} bisadduct (ICBA), used extensively as an acceptor in polymer solar cells, increases the open-circuit voltage (V_{OC}) because of the higher energy level of the lowest unoccupied molecular orbital (LUMO) of ICBA, thereby increasing the PCE;[31] this situation does not occur often in OSCs when using polymers of low band gap. Although the values of V_{OC} will increase when incorporating ICBA as an acceptor in low-band-gap polymer-based solar cells, the short-circuit current densities (J_{SC}) and fill factor (FF) will decrease significantly.[32] The similar observation are also reported by Nguyen et al while solution-processed small molecule donor DTS($FBTTh_2$)$_2$:$PC_{71}BM$ replacing by ICBA shows the lower J_{SC} and FF.[33] Recently, Cheng et al. reported efficient ternary polymer solar cells incorporating ICBA as a cascade acceptor in a blend of poly(4,8-bis[(2-ethylhexyl)oxy]benzo[1,2-*b*:4,5-*b*′]dithiophene-2,6-diyl-*alt*-3-fluoro-2-[(2-ethylhexyl)carbonyl]thieno[3,4-*b*]thiophene-4,6-diyl) (PTB7) and $PC_{71}BM$. The efficiencies of these ternary cascade polymer solar cells are much higher than those of both PTB7/$PC_{71}BM$- and PTB7/ICBA-based solar cells.[34]

In this paper, we report efficient ternary BHJ solar cells prepared using all small molecules—namely (2*Z*,2′*E*)-dioctyl 3,3′-(5′′,5′′′′′-(4,8-bis(5-octylthiophen-2-yl)benzo[1,2-*b*:5,4-*b*′]dithiophene-2,6-diyl) bis(3,4′,4′′-trioctyl-[2,2′:5′,2′′-terthiophene]-5′′,5-diyl))bis(2-cyanoacrylate)

(BDT6T), ICBA, and $PC_{71}BM$. The appropriate energy level of ICBA, positioned between those of BDT6T and $PC_{71}BM$, forms a cascade energy level structure that facilitates exciton dissociation and provides more routes for charge transfer. Meanwhile, the morphologies of such BHJ films changed significantly, resulting in different scenarios for exciton dissociation and charge carrier transport. With the optimized weight ratio of BDT6T, ICBA, and $PC_{71}BM$, the PCE increased from 5.61% to 6.36%.

2. Experimental

The synthesis of BDT6T, used as the donor material, has been described previously.[35] The active layer solutions for the binary and ternary blends comprised BDT6T (8 mg mL^{-1} in $CHCl_3$) and $PC_{71}BM$ (Solenne BV), with the latter replaced by various ratios of ICBA (Solenne BV) in $PC_{71}BM$. The chemical structures of BDT6T, ICBA, and $PC_{71}BM$ are displayed in Fig. 1. To investigate the effect of ICBA concentration on the device performance, the overall ratio of the small molecule to the fullerene derivative in each device was maintained at 1:0.4 while varying the composition of the fullerene (i.e., varying the ICBA-to-$PC_{71}BM$ ratio). Prior to device fabrication, the patterned ITO glasses (<7 Ω sq^{-1}; active area: 0.1 cm^2) were cleaned in detergent, DI water, acetone, and isopropyl alcohol. After routine solvent cleaning, the ITO substrates were treated with UV ozone for 15 min, spin-coated (4000 rpm, 60 s) with PEDOT: PSS as the hole collection layer, and baked (130°C, 30 min). The active layer solution (BDT6T:$PC_{71}BM$ or BDT6T:ICBA:$PC_{71}BM$) was then spin-coated (3000 rpm, 60 s) onto the PEDOT: PSS-modified ITO substrate. Finally, 30- and 60-nm-thick layers of Ca and Al were thermally evaporated through a shadow mask inside a vacuum chamber (<6×10^{-6} torr). In the hole-only and electron-only devices, Ca was replaced by V_2O_5, because its higher work function (Φ= 5.3 eV)

provided a better hole injection contact for the active layer. A layer thickness of 10 nm V_2O_5 was thermally evaporated and then it was capped with a layer of Al (100 nm). For the electron-only devices, the PEDOT: PSS layer was replaced with Cs_2CO_3 (Φ= 2.9 eV), which is an efficient electron injection layer.

A Jacobs V-670 UV–Vis–NIR spectrophotometer was used to measure the absorption spectra of the active layer films. A Bruker Innova atomic force microscope (AFM, Digital Instrument NS 3a controller equipped with a D3100 stage) was used, in the tapping mode, to record the surface morphologies of the active layers. Prior to characterization using transmission electron microscopy (TEM, JEM 2100F), the active layer on a PEDOT:PSS substrate was removed by dipping in DI water and then a holey carbon-coated copper grid (Ultrathin Carbon Type-A, 400 mesh, Copper; TED Pella) was used to hold the film, which was dried in an oven at 50 °C. The photovoltaic performance of each device was measured under simulated AM 1.5 G illumination (100 mW cm^{-2}) using a Xe lamp–based solar simulator (Thermal Oriel 1000 W) inside a N_2-filled glove box. The light intensity was calibrated using a mono-silicon photodiode and a KG-5 color filter (Hamamatsu). Photoluminescence (PL) and femtosecond time-resolved PL (TRPL) were used to measure the emission spectra and fluorescence dynamics processes, respectively, of the blend films. For TRPL, a Ti: sapphire laser operated at λ = 840 nm, with repetition rate of 80 MHz, pulse duration Δt = 100 fs, and average power of 1 W, was used as the pump. A BBO crystal was used to convert the photon energy of the pump from 1.478 eV (λ = 840 nm) to 2.956 eV (λ = 420 nm). The converted pulse (λ = 420 nm) was then guided to excite the blended film, and the residual pump was used to temporally resolve the luminescence by a computer-controlled delay stage. To prevent laser-induced degradation, the diameter of the spot size of the excitation on the sample was expanded to 300 μm and the average excitation power was reduced to 4 mW. In our

system, the instrument response is about 150 fs.[36] Impedance spectra were measured through frequency response analysis using a Metrohm Autolab apparatus.

3. Results and discussion

Fig. 1 displays the energy levels of the highest occupied molecular orbitals (HOMOs) and LUMOs of BDT6T, ICBA and $PC_{71}BM$.[34] The energy band edges of ICBA are intermediate between those of BDT6T and $PC_{71}BM$ and also provided sufficiently large band edge offsets with BDT6T for exciton dissociation. With such appropriately aligned HOMO and LUMO energy levels we expected carriers to be driven forward along the energy cascades with minimized recombination. Meanwhile, we expected the value of V_{OC} to increase for devices based on this ternary blend upon increasing the amount of ICBA.

Fig. 2(a) displays the *J*–*V* characteristics of BDT6T:ICBA:$PC_{71}BM$ devices incorporating 0, 15, and 40% of ICBA. The device performance of the binary BHJ solar cell was characterized by a value of J_{SC} of 10.70 mA cm^{-2}, a value of V_{OC} of 0.92 V, and an FF of 0.57, corresponding to a PCE of 5.61%. Increasing the ICBA ratio to 15% provided a ternary BHJ solar cell exhibiting higher performance than that of the binary cell. The values of J_{SC} and V_{OC} increased to 12.00 mA cm^{-2} and 0.93 V, respectively, with the same FF of 0.57, leading to a PCE of 6.36%—an increase of 13% relative to that of the binary device. Increasing the ratio of ICBA to 40% caused the value of V_{OC} to increase further to 0.95 V, but the value of J_{SC} and the FF both decreased accordingly, leading the lower cell performance (PCE = 4.57%). Table 1 and Fig. S2 summarize these parameters and the *J*–*V* characteristics of the devices incorporating the different ICBA ratios. We calculated the average PCEs from 10 devices fabricated in two different batches. The value of V_{OC} increased upon increasing the ratio of ICBA because of the higher LUMO energy level than

$PC_{71}BM$.[30] The value of J_{SC} and the FF began to decrease when the content of ICBA was greater than 20%; hence, the PCE increased initially upon increasing the content of ICBA, but decreased after a certain content had been reached. The external quantum efficiency (EQE) spectra at a given wavelength reflect the light response of a device, and are related directly to the values of J_{SC}. The EQE spectra of the binary and ternary devices in Figure 2(b) reveal photocurrent responses in the wavelength range from 300 to 700 nm. The EQE of the ternary device based on BDT6T:ICBA (15%):$PC_{71}BM$ was higher than that of the binary device in the full-scale visible region. The calculated J_{SC} integrated from the EQE spectrum for the binary and ternary (15% and 40% ICBA) device is 10.58, 11.93 and 9.35 $mA \cdot cm^{-2}$, respectively, in agreement with the measured values from the *J–V* curves.

We used UV–Vis spectroscopy to study the change in absorption following incorporation of the third component [Fig. 2(c)]. The main absorption range of the BDT6T:$PC_{71}BM$ film was between 400 and 700 nm, with the maximum absorption peak located at 570 nm. The absorption intensity decreased upon increasing the ratio of ICBA in the fullerene, due to the absorption strength of ICBA being less than that of $PC_{71}BM$ in the visible region. Nevertheless, the location of the vibronic peak (ca. 628 nm) remained unchanged after blending in the ICBA, implying that the packing structure of BDT6T was not affected significantly in the ternary blend. Thus, the increase in photocurrent could not be attributed to any change in absorption after adding 15% ICBA to the fullerene.

To study the cause of the improved J_{SC} of the devices, we recorded static and dynamic PL spectra to investigate the photoinduced charge transfer between the donor and acceptor. Fig. 3(a) displays PL spectra of films of pristine BDT6T and BDT6T:$PC_{71}BM$ and BDT6T:$PC_{71}BM$:ICBA (15%) blends. The PL spectrum of

pristine BDT6T features a maximum emission at 733 nm; for the binary and ternary blend films, these PL emissions were quenched significantly, with the ternary blend film having greater PL quenching capability than the binary film. This behavior suggested that efficient charge transfer of the ternary blend film is due to the better mixing between the donor and acceptor phases. We used TRPL to study the fluorescence dynamics processes for films of pristine BDT6T and BDT6T:$PC_{71}BM$ and BDT6T:$PC_{71}BM$: ICBA (15%) blends [Fig. 3(b)]. We obtained the time constants for exciton dissociation (τ_1) and exciton diffusion (τ_2) by fitting with two-exponential decay functions. The value of τ_1 for the BDT6T:$PC_{71}BM$:ICBA (15%) film (0.85 ps) was slightly faster than that (0.89 ps) for the BDT6T:$PC_{71}BM$ film, indicating that the ICBA in the ternary blend film reveals better intermixing leading to the faster charge transfer kinetics. The value of τ_2 for the BDT6T:$PC_{71}BM$:ICBA (15%) film (12.42 ps) was shorted than that (14.71 ps) for the BDT6T:$PC_{71}BM$ film. Because the exciton diffusion time correlated with the degree of mixing in the blend film, we wished to further investigate the morphological changes in the binary and ternary systems.

Fig. 4 presents AFM height images of BDT6T:ICBA:$PC_{71}BM$ films incorporating different ratios of ICBA. The morphology of the BDT6T:$PC_{71}BM$ film featured many aggregated domains, with a root-mean-square (RMS) roughness of 1.2 nm. After incorporating 15% of ICBA into $PC_{71}BM$, the domain size decreased and the film became smoother (RMS roughness: 0.71 nm), suggesting that additional interfaces had been generated between the donor and acceptor. Further increasing the ratio of ICBA to 40 and 100% caused the surface morphologies [Figs. 4(c) and 4(d), respectively] to become even more homogeneous and smooth, resulting in destruction of the continuous channels for charge transport and leading to decreases in the values of J_{SC}, FF, and PCE. To understand the effect of ICBA on the film morphologies, we measured the contact angle of each material and calculated its surface energy (γ) using

the equation of state: [37] $1 + \cos\theta = 2 \cdot \sqrt{\frac{\gamma_s}{\gamma_l}} \cdot e^{-\beta(\gamma_l - \gamma_s)^2}$ where γ_l is surface tension of liquid, γ_s is surface energy of material and the value of β (0.0001247) is determined empirically. Accordingly, we estimated the surface energies of BDT6T, ICBA, and $PC_{71}BM$ to be 26.2, 27.4, and 30.3 mJ m^{-2}, respectively. The relatively small value of $|\Delta\gamma|$ between BDT6T and ICBA leads to well-mixed films because of the lower thermodynamic driving force for phase separation. As a result, the presence of ICBA in the ternary system led to the generation of additional interfaces in the active layer. To obtain further insight into the morphology of the active layer, we recorded high-resolution TEM images of films of the binary and ternary blends [Figs. 4(e) and 4(f), respectively]. We presume that the bright and dark regions represent the donor- and acceptor-rich domains, respectively, because fullerene derivatives typically appear darker in TEM images because their electron density is higher than that of BDT6T.[38] The film of the BDT6T:$PC_{71}BM$:ICBA (15%) ternary blend featured the fine features of phase separation while retaining the interpenetrating network, thereby allowing more heterojunction interfaces to be produced for the efficient dissociation of excitons and more carriers to be collected by the electrodes. As would be expected for a device exhibiting increased exciton dissociation and a superior carrier transport pathway, we observed a corresponding increase in current density. In contrast, the BDT6T:$PC_{71}BM$ film featured relatively large donor- and acceptor-rich domains, which appeared as isolated domains in the active layer; such isolated domains would encourage carrier recombination. Therefore, an appropriate amount of ICBA induced finer phase separation while maintaining continuous pathways in the BHJs, thereby enhancing photocurrent generation.

To gain more insight into the morphological changes and electrical properties of our devices, we used impedance spectroscopy to investigate the organic–organic

interfaces in the active layer. Fig. 5(a) displays the equivalent circuit model correlated to the BHJ solar cells. R1 and C1 in the circuit model refer to the combination of recombination resistance and chemical capacitance of each interface between donors and acceptors, respectively, in the BHJ layer;[39] R2 and C2 correspond to these values at the interface between the active layer and the electrode; R3 represents the resistance from the electrodes. The impedance spectra measured at frequencies from 100 Hz to 1 MHz revealed complex plots comprising the resistance and reactance. The Cole–Cole plot in Fig. 5(b) is not a perfect semicircle; it comprises a large semicircle at low frequency and a small semicircle at high frequency. Table 2 lists the fitted values of each element. The capacitance C1 increased from 0.548×10^{-7} to 0.665×10^{-7} F upon increasing the ratio of ICBA in the fullerene; simultaneously; the resistance R1 decreased from 306.7 to 238.5Ω. Thus, the interfacial area between the donor and acceptor increased upon the blending of ICBA, leading to enhanced capacitance and decreased resistance. Our observation is similar to that reported previously after blending different concentrations of additives into active layers to enhance the interfacial area between the donor and acceptor.[40] The effective carrier lifetime can be obtained from the equation

$$\tau = C \times R$$

The carrier lifetime (1.80×10^{-5} s) of the ternary blend film (15% ICBA) was longer than that of the binary blend (1.68×10^{-5} s), suggesting that the carriers in the ternary blend film had better opportunity to reach their electrodes. The carrier lifetime (1.58×10^{-5} s) of the ternary blend film incorporating 40% ICBA decreased because the surplus of interfaces led to greater carrier recombination.

The space-charge limited current (SCLC) model was used to determine the carrier mobility. Fig. S3 shows the *J*–*V* characteristics of the electron and hole-only devices. Based on the fitting of the dark current by the SCLC model, $J = 9\varepsilon_0\varepsilon_r\mu V^2/$

$8L^3$,[41] the electron and hole mobilities for BDT6T:$PC_{71}BM$ are determined to be 1.20×10^{-8} and 9.13×10^{-9} m^2/V-s, respectively. After blending 15% ICBA, the electron mobility of ternary blend film remains similarly about 1.12×10^{-8} m^2/V-s and hole mobility increased to 1.27×10^{-8} m^2/V-s. The electron and hole mobilities after blending 40% IBCA decreased to 7.90×10^{-9} and 6.77×10^{-9} m^2/V-s, respectively. The results indicated that the optimized amount of ICBA in the ternary blend film not only generates more heterojunction interfaces, but also maintains continuous pathways for effective charge transport. Excessive amount of ICBA in the active layer shows uniform intermixing which is not favorable for charge transport.

4. Conclusion

We have demonstrated efficient ternary SMOSCs featuring ICBA as a cascade acceptor in BDT6T:$PC_{71}BM$ blends. ICBA not only has an energy level appropriately balanced between those of its blend counterparts, thereby establishing more charge transfer routes, but it also has a surface energy similar to that of BDT6T, allowing for manipulation of the morphologies of its blend film. By optimizing the amount of added ICBA, we established an interface exhibiting enhanced interpenetration between BDT6T and the fullerene derivatives, relative to that formed in the binary system, leading to significantly suppressed carrier recombination in isolated domains and increased carrier extraction. As a result, the PCE of the optimized device increased considerably, to 6.36%. Our findings suggest great promise for achieving efficient BHJ SMOSCs through the use of ternary blends.

Acknowledgment

C.-W.C thanks the Taiwan Ministry of Science and Technology (102-2221-E-001-029 -MY2), the Center for Sustainability Science of Academia Sinica, Taiwan (AS-103-SS-A02), and Academia Sinica, Taiwan (Career Development Award 103-CDA-M01), for financial support. We thank NanoCore, the Core Facilities for Nanoscience and Nanotechnology at Academia Sinica, Taiwan, for technical support.

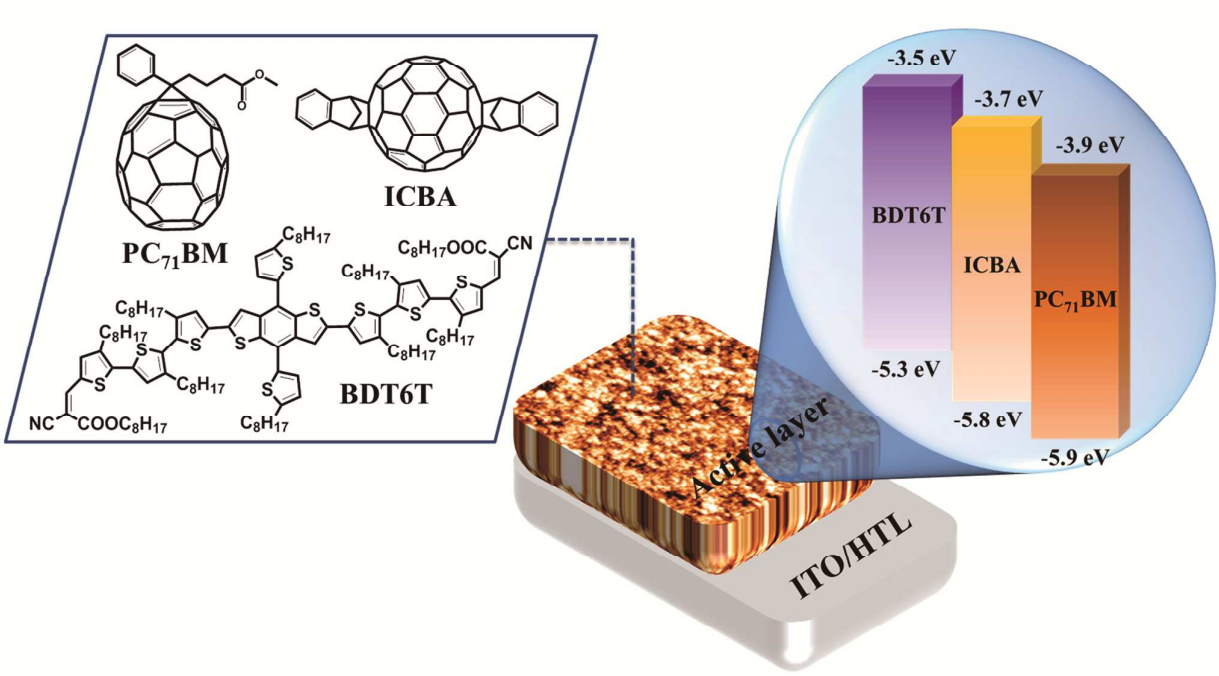

Fig. 1 Chemical structures and energy levels of BDT6T, $PC_{71}BM$, and ICBA.

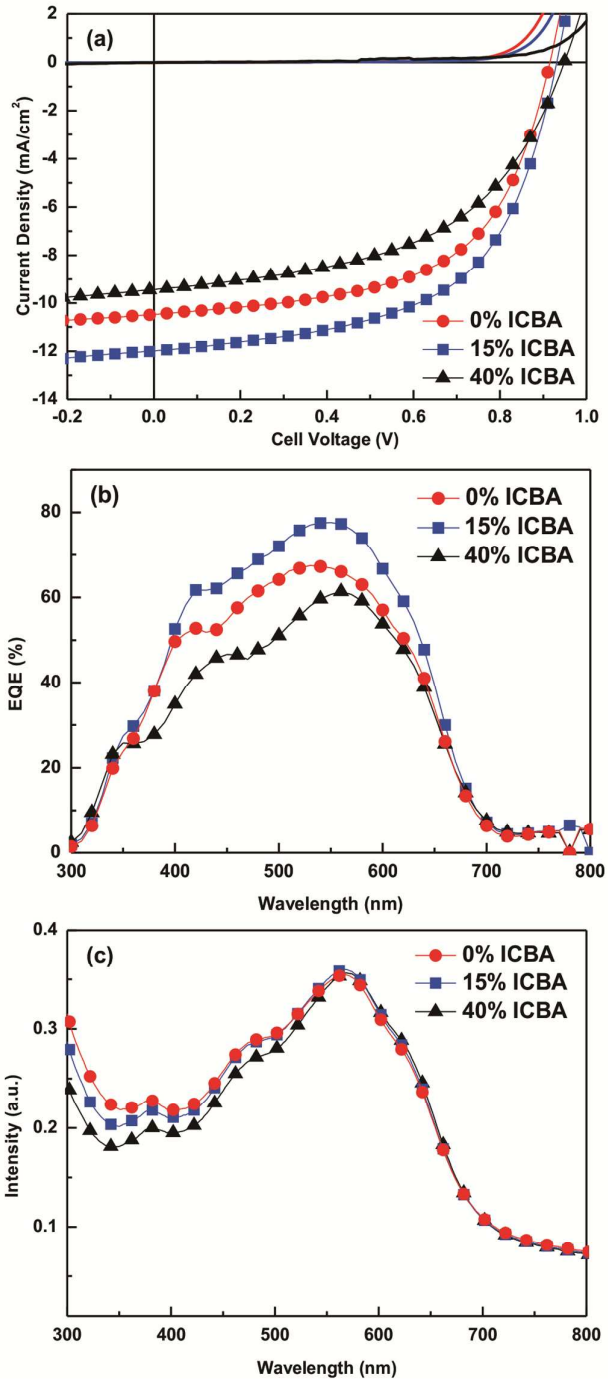

Fig. 2 (a) *J–V* curves and (b) EQE spectra of devices incorporating different ratios of ICBA, under illumination. (c) UV–Vis absorption spectra of BDT6T:ICBA:$PC_{71}BM$ films incorporating 0, 15, and 40% ICBA in the active layer.

Table. 1 Performance characteristics of devices based on BDT6T:ICBA:$PC_{71}BM$ blend films

ICBA (%)	V_{OC} (V)	J_{SC} (mA cm^{-2})	FF	PCE (%)	
				Average	Best
0%	0.92	10.70	0.57	5.61	5.74
10%	0.92	11.70	0.57	6.13	6.23
15%	0.93	12.00	0.57	6.36	6.43
20%	0.93	11.50	0.56	5.99	6.14
40%	0.95	9.44	0.51	4.57	4.71
100%	1.00	6.34	0.45	2.85	2.97

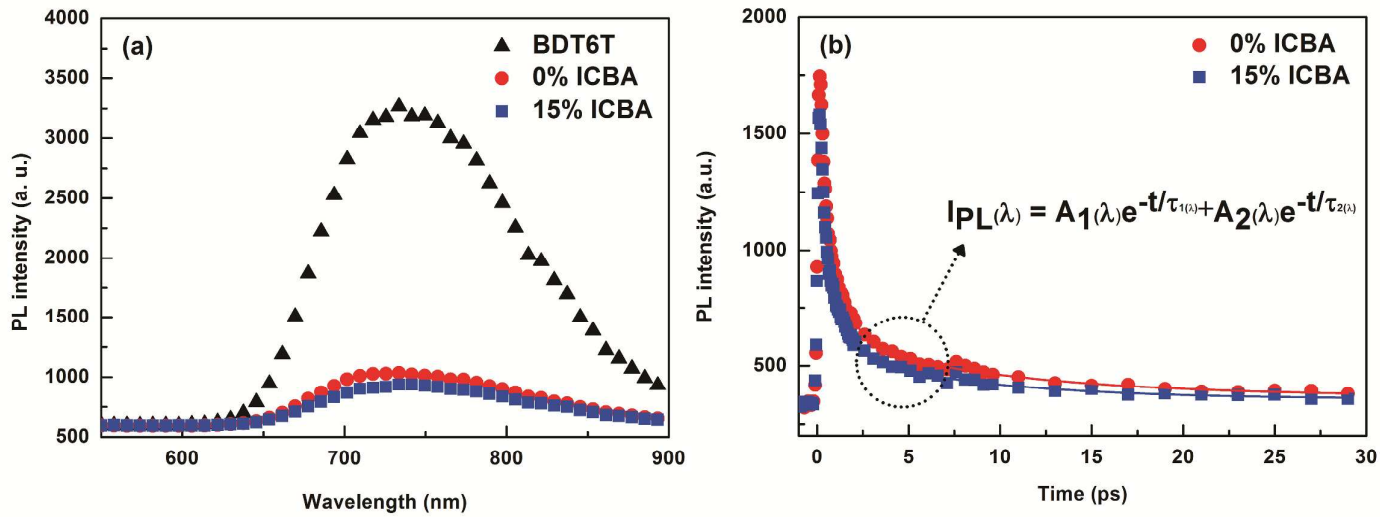

Fig. 3 (a) PL spectra of films of BDT6T, BDT6T:$PC_{71}BM$, and BDT6T:ICBA (15%):$PC_{71}BM$. (b) TRPL spectra of BDT6T:ICBA:$PC_{71}BM$ films incorporating 0 and 15% ICBA on PEDOT:PSS/ITO substrates and the decay was measured at 730 nm.

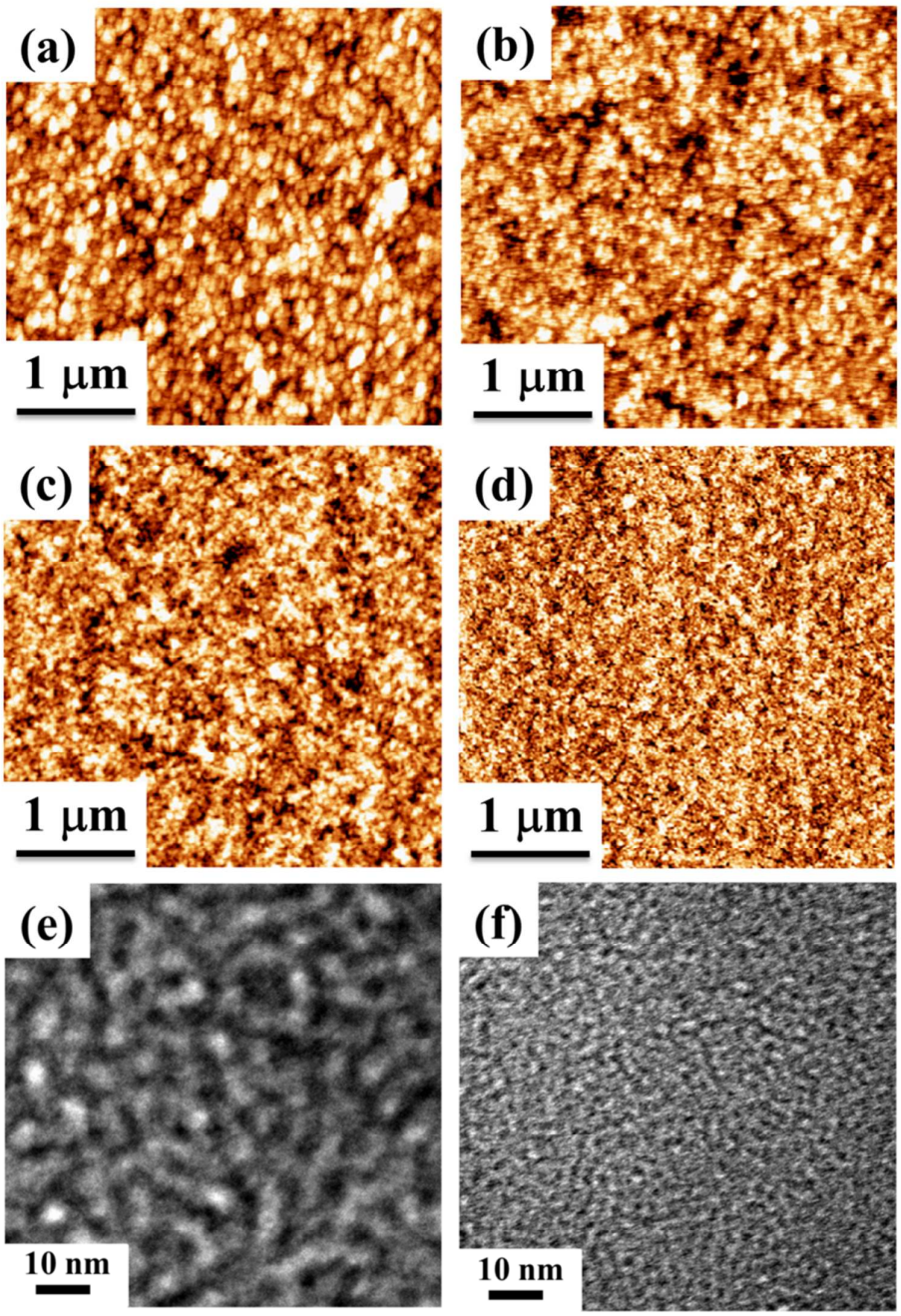

Fig. 4 (a–d) AFM height images of BDT6T:ICBA:$PC_{71}BM$ active layer films featuring (a) 0, (b) 15, (c) 40, and (d) 100% ICBA in the fullerene on PEDOT:PSS/ITO substrates. (e, f) TEM images of BDT6T:ICBA:$PC_{71}BM$ films incorporating (e) 0 and (f) 15% ICBA in the fullerene.

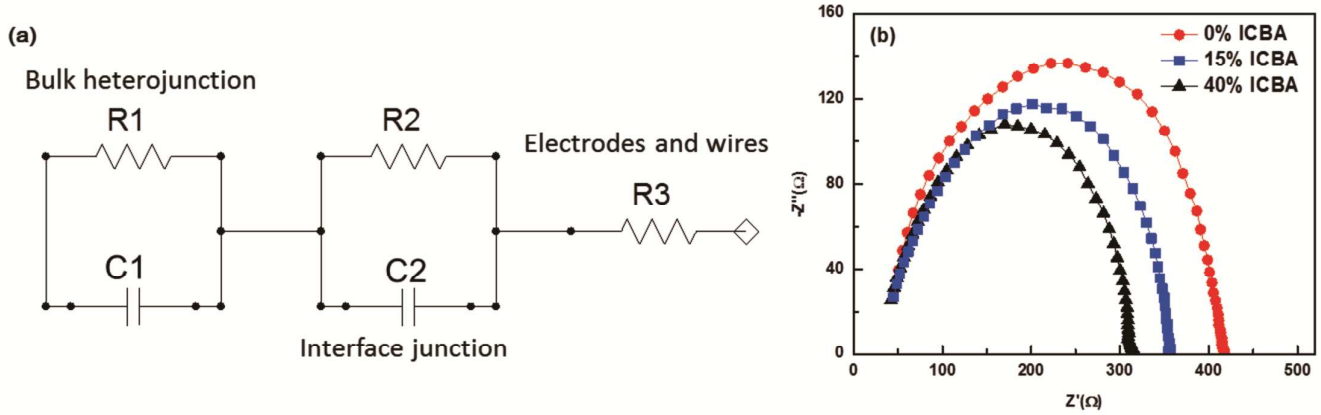

Fig. 5 (a) Equivalent circuit model of the devices. (b) Cole–Cole plots of the devices incorporating 0, 15, and 40% ICBA in the fullerene.

Table. 2 Resistances, capacitances, and carrier lifetimes fitted from the equivalent model for BDT6T:ICBA:$PC_{71}BM$ devices incorporating various ratios of ICBA

ICBA (%)	R1 (Ω)	C1 (F)	R2 (Ω)	C2 (F)	R3 (Ω)	τ (s)
0%	306.7	0.548×10^{-7}	71.7	0.760×10^{-8}	38.3	1.68×10^{-5}
15%	276.9	0.651×10^{-7}	40.8	0.121×10^{-7}	38.9	1.80×10^{-5}
40%	238.5	0.665×10^{-7}	34.1	0.148×10^{-7}	38.5	1.58×10^{-5}

References

1. G. Li, R. Zhu and Y. Yang, *Nat Photon*, 2012, **6**, 153-161.
2. A. Facchetti, *Chem. Mater.*, 2010, **23**, 733-758.
3. L.-M. Chen, Z. Hong, G. Li and Y. Yang, *Adv. Mater.*, 2009, **21**, 1434-1449.
4. C. R. McNeill and N. C. Greenham, *Adv. Mater.*, 2009, **21**, 3840-3850.
5. S. Sista, Z. Hong, L.-M. Chen and Y. Yang, *Energy Environ. Sci.*, 2011, **4**, 1606-1620.
6. Z. He, B. Xiao, F. Liu, H. Wu, Y. Yang, S. Xiao, C. Wang, T. P. Russell and Y. Cao, *Nat Photon*, 2015, DOI: 10.1038/nphoton.2015.6
7. Y. Liu, J. Zhao, Z. Li, C. Wu, W. Ma, H. Hu, K. Jiang, H. Lin, H. Ade and H. Yan, *Nat Commun.*, 2014, **5**, 6293.
8. H. Zhou, Y. Zhang, C. -K. Mai, S. D. Collins, G. C. Bazan, T. -Q. Nguyen and A. J. Heeger, *Adv. Mater.*, 2015, DOI: 10.1002/adma.201404220
9. A. R. b. M. Yusoff, D. Kim, H. P. Kim, F. K. Shneider, W. J. da Silva and J. Jang, *Energy Environ. Sci.*, 2015, **8**, 303-316.
10. A. Mishra and P. Bäuerle, *Angew. Chem. Int. Ed.*, 2012, **51**, 2020-2067.
11. Y. Sun, G. C. Welch, W. L. Leong, C. J. Takacs, G. C. Bazan and A. J. Heeger, *Nat Mater*, 2012, **11**, 44-48.
12. M. T. Lloyd, A. C. Mayer, S. Subramanian, D. A. Mourey, D. J. Herman, A. V. Bapat, J. E. Anthony and G. G. Malliaras, *J. Am. Chem. Soc.*, 2007, **129**, 9144-9149.
13. F. Silvestri, A. Marrocchi, M. Seri, C. Kim, T. J. Marks, A. Facchetti and A. Taticchi, *J. Am. Chem. Soc.*, 2010, **132**, 6108-6123.
14. B. Walker, A. B. Tamayo, X.-D. Dang, P. Zalar, J. H. Seo, A. Garcia, M. Tantiwiwat and T.-Q. Nguyen, *Adv. Funct. Mater.*, 2009, **19**, 3063-3069.
15. J. Zhou, Y. Zuo, X. Wan, G. Long, Q. Zhang, W. Ni, Y. Liu, Z. Li, G. He, C. Li, B. Kan, M. Li and Y. Chen, *J. Am. Chem. Soc.*, 2013, **135**, 8484-8487.
16. A. K. K. Kyaw, D. H. Wang, V. Gupta, J. Zhang, S. Chand, G. C. Bazan and A. J. Heeger, *Adv. Mater.*, 2013, **25**, 2397-2402.
17. D. Yang, Q. Yang, L. Yang, Q. Luo, Y. Chen, Y. Zhu, Y. Huang, Z. Lu and S. Zhao, *Chem. Commun.*, 2014, **50**, 9346-9348.
18. J. Zhou, X. Wan, Y. Liu, Y. Zuo, Z. Li, G. He, G. Long, W. Ni, C. Li, X. Su and Y. Chen, *J. Am. Chem. Soc.*, 2012, **134**, 16345-16351.
19. C. Waldauf, M. Morana, P. Denk, P. Schilinsky, K. Coakley, S. A. Choulis and C. J. Brabec, *Appl. Phys. Lett.*, 2006, **89**, 233517.
20. J. H. Seo, A. Gutacker, Y. Sun, H. Wu, F. Huang, Y. Cao, U. Scherf, A. J. Heeger and G. C. Bazan, *J. Am. Chem. Soc.*, 2011, **133**, 8416-8419.
21. X. Wan, Y. Liu, F. Wang, J. Zhou, G. Long and Y. Chen, *Org. Electron.*, 2013,

14, 1562-1569.

22. T. Ameri, T. Heumuller, J. Min, N. Li, G. Matt, U. Scherf and C. J. Brabec, *Energy Environ. Sci.*, 2013, **6**, 1796-1801.
23. T. Ameri, J. Min, N. Li, F. Machui, D. Baran, M. Forster, K. J. Schottler, D. Dolfen, U. Scherf and C. J. Brabec, *Adv. Energy Mater.*, 2012, **2**, 1198-1202.
24. S.-Y. Chang, H.-C. Liao, Y.-T. Shao, Y.-M. Sung, S.-H. Hsu, C.-C. Ho, W.-F. Su and Y.-F. Chen, *J. Mater. Chem. A*, 2013, **1**, 2447-2452.
25. Q. An, F. Zhang, L. Li, J. Wang, J. Zhang, L. Zhou and W. Tang, *ACS Appl. Mater. Interfaces*, 2014, **6**, 6537-6544.
26. J. A. Mikroyannidis, D. V. Tsagkournos, S. S. Sharma, A. Kumar, Y. K. Vijay and G. D. Sharma, *Sol. Energy Mater. Sol. Cells*, 2010, **94**, 2318–2327.
27. T. Rousseau, A. Cravino, T. Bura, G. Ulrich, R. Ziessel and J. Roncali, *J. Mater. Chem.*, 2009, **19**, 2298–2300.
28. J. N. de Freitas, I. R. Grova, L. C. Akcelrud, E. Arici, N. S. Sariciftci and A. F. Nogueira, *J. Mater. Chem.*, 2010, **20**, 4845-4853.
29. G. Itskos, A. Othonos, T. Rauch, S. F. Tedde, O. Hayden, M. V. Kovalenko, W. Heiss and S. A. Choulis, *Adv. Energy Mater.*, 2011, **1**, 802-812.
30. P. P. Khlyabich, B. Burkhart and B. C. Thompson, *J. Am. Chem. Soc.*, 2011, **133**, 14534-14537.
31. Y. He, H.-Y. Chen, J. Hou and Y. Li, *J. Am. Chem. Soc.*, 2010, **132**, 1377-1382.
32. J.-H. Huang, Y.-S. Hsiao, E. Richard, C.-C. Chen, P. Chen, G. Li, C.-W. Chu and Y. Yang, *Appl. Phys. Lett.*, 2013, **103**, 043304.
33. A. K. K. Kyaw, D. Gehrig, J. Zhang, Y. Huang, G. C. Bazan, F. Laquai and T.-Q. Nguyen, *J. Mater. Chem. A*, 2015, 3, 1530–1539.
34. P. Cheng, Y. Li and X. Zhan, *Energy Environ. Sci.*, 2014, **7**, 2005-2011.
35. D. Patra, T.-Y. Huang, C.-C. Chiang, R. O. V. Maturana, C.-W. Pao, K.-C. Ho, K.-H. Wei and C.-W. Chu, *ACS Appl. Mater. Interfaces*, 2013, **5**, 9494-9500.
36. S. H. Chang, C. -H. Chiang, H.-M. Cheng, C.-Y. Tai and C. -G. Wu, *Opt. Lett*, 2013, **38**, 5342-5345.
37. D. Li and A. W. Neumann, *Adv. Colloid Interface Sci.*, 1992, **39**, 299-345.
38. Y. Liu, C.-C. Chen, Z. Hong, J. Gao, Y. Yang, H. Zhou, L. Dou, G. Li and Y. Yang, *Sci. Rep.*, 2013, **3**.
39. J. Bisquert, *Phys. Chem. Chem. Phys.*, 2003, **5**, 5360-5364.
40. E.-P. Yao, C.-C. Chen, J. Gao, Y. Liu, Q. Chen, M. Cai, W.-C. Hsu, Z. Hong, G. Li and Y. Yang, *Sol. Energy Mater. Sol. Cells*, 2014, **130**, 20-26.
41. P. Mark and W. Helfrich, *J. Appl. Phys.*, 1962, **33**, 205.

Graphical Abstract

Efficient Ternary Bulk Heterojunction Solar Cells Based on Small Molecules Only

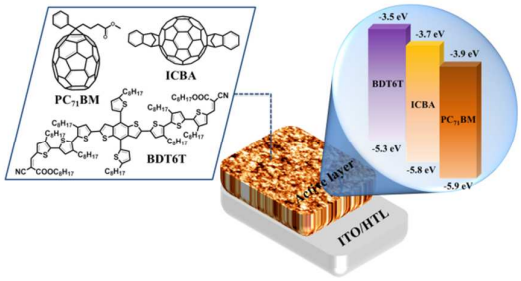

Efficient ternary BHJ solar cells fabricated using small molecules—namely BDT6T, ICBA, and $PC_{71}BM$ achieving a PCE of 6.36%.